Supporting Information

Tailoring Composition and Material Distribution in Multicomponent Cryoaerogels for Application in Photocatalysis

Axel Freytag[†,‡], Carsten Günnemann[†,‡], Suraj Naskar[†,‡], Saher Hamid[§,‡,¶], Franziska Lübkemann[†,‡], Detlef Bahnemann[§,‡,¶], Nadja C. Bigall[†,‡]*

† Institute of Physical Chemistry and Electrochemistry (PCI), Leibniz Universität Hannover, Callinstraße 3A, D-30167 Hannover, Germany

‡ Laboratory of Nano and Quantum Engineering (LNQE), Leibniz Universität Hannover, Schneiderberg 39, D-30167 Hannover, Germany

§ Institute for Technical Chemistry, Leibniz Universität Hannover, Callinstraße 3, D-30167 Hannover, Germany

¶ Laboratory "Photoactive Nanocomposite Materials", Saint-Petersburg State University, Ulyanovskaya str. 1, Peterhof, Saint-Petersburg, 198504, Russia

* nadja.bigall@pci.uni-hannover.de

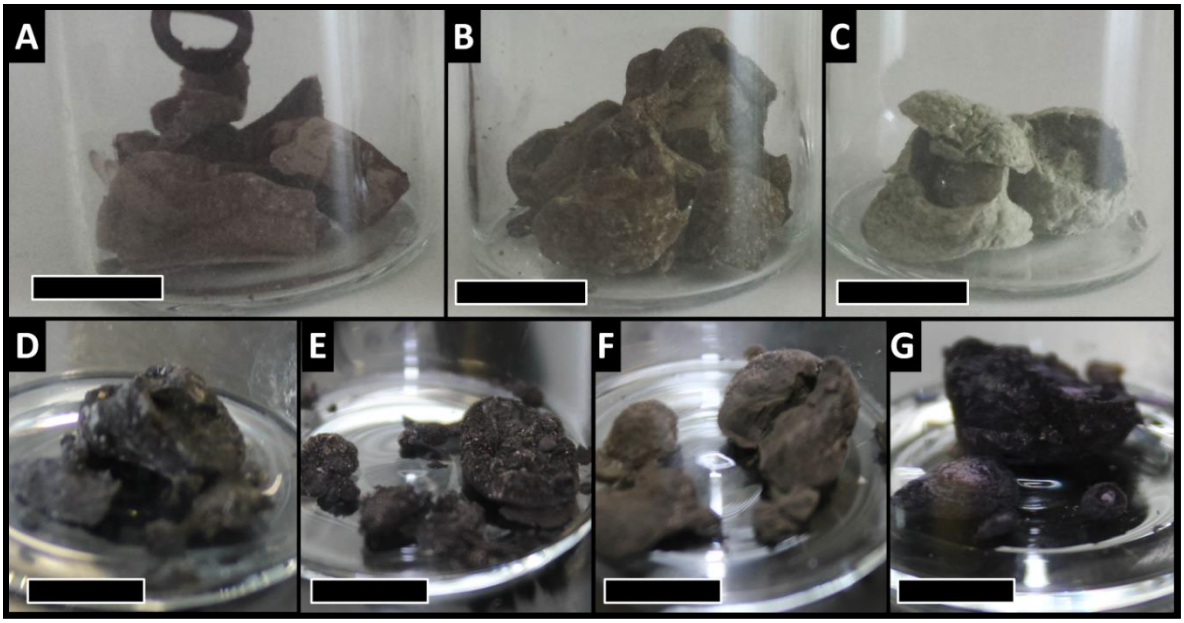

Figure S1. Various cryoaerogelated monoliths from mixed systems. Cryoaerogel of (A) $MnO(OH)_x$-Pt (1wt%), (B) $CoO(OH)_x$-Pt (1wt%), (C) $NiO(OH)_x$-Pt (1wt%), (D) hematite-Ag (50wt%), (E) hematite-Au (50wt%), (F) titania-Ag (50wt%) and (G) titania-Au (50wt%) were synthesized. The scale bar corresponds to 1 cm.

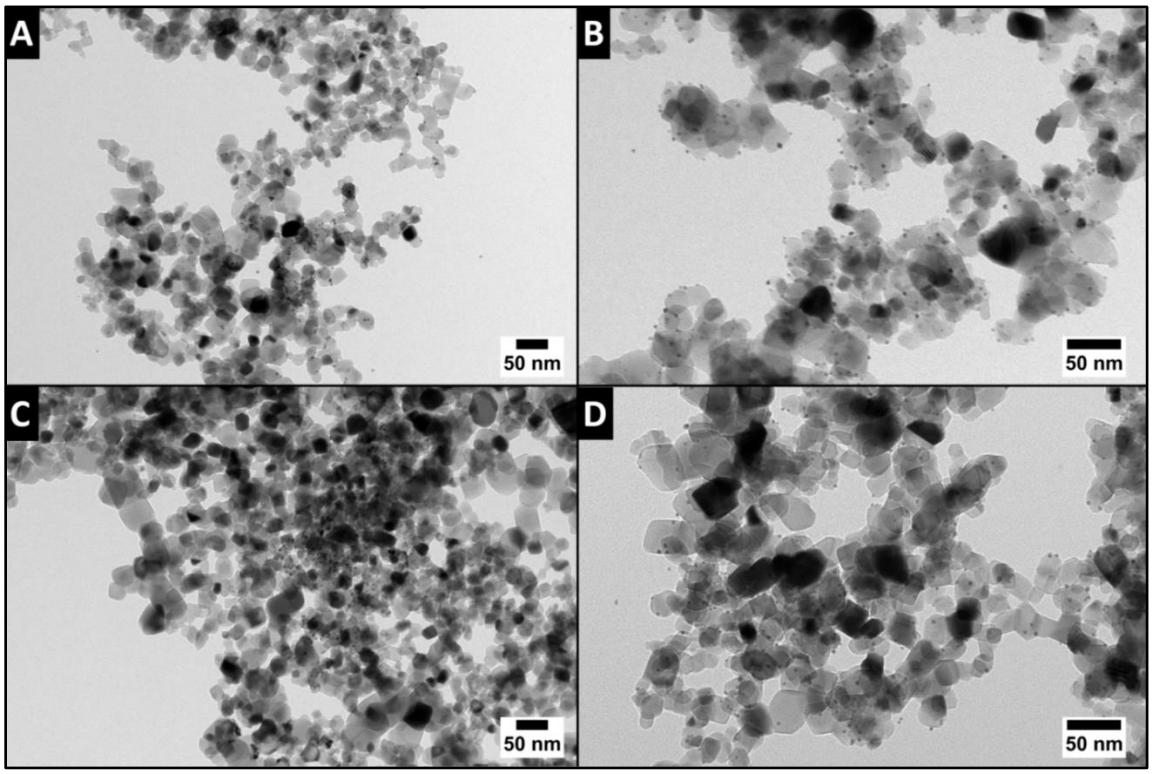

Figure S2. TEM images of the system TiO_2-Pt (1 wt%) showing samples prepared from (A) the colloidal solution with same ζ-potential for both components, (B) the colloidal solution with opposite ζ-potential

for both components, (C) the cryoaerogel with same ζ-potential for both components, and (D) the cryoaerogel with opposite ζ-potential for both components. Note, that for the colloidal solution drying effects might occur during the TEM preparation.

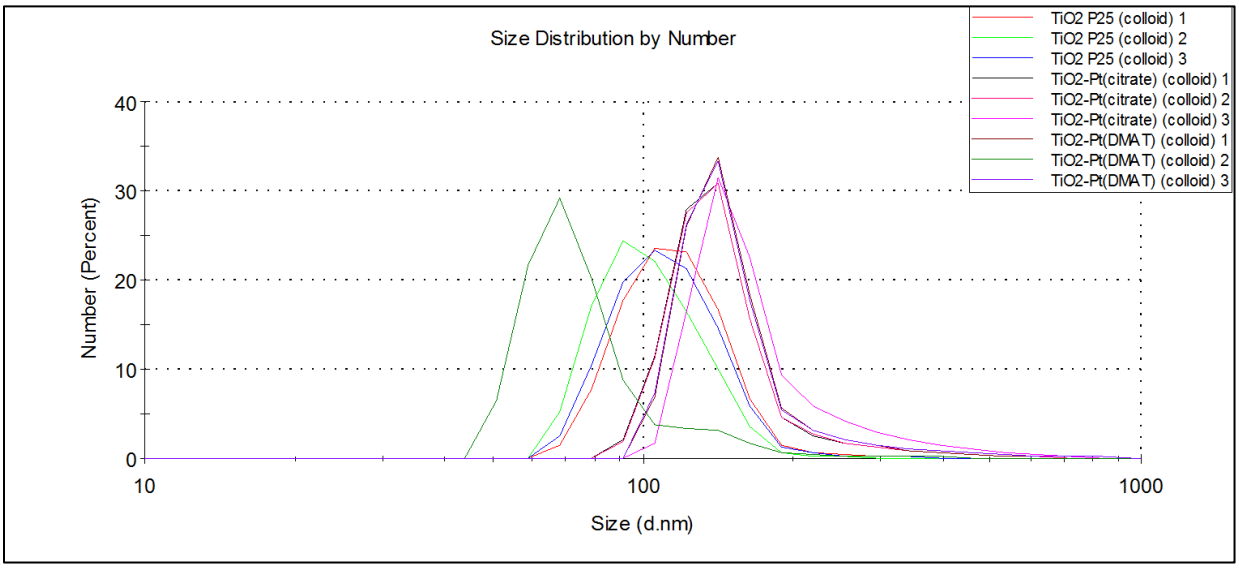

Figure S3. DLS measurements of the system TiO_2-Pt (1 wt%) of the pure TiO_2 nanoparticles (in the caption TiO2 P25 1, 2, and 3, respectively) and the mixtures immediately after addition of Pt nanoparticles of similar ζ-potential (DMAT) and of opposite ζ-potential (citrate).

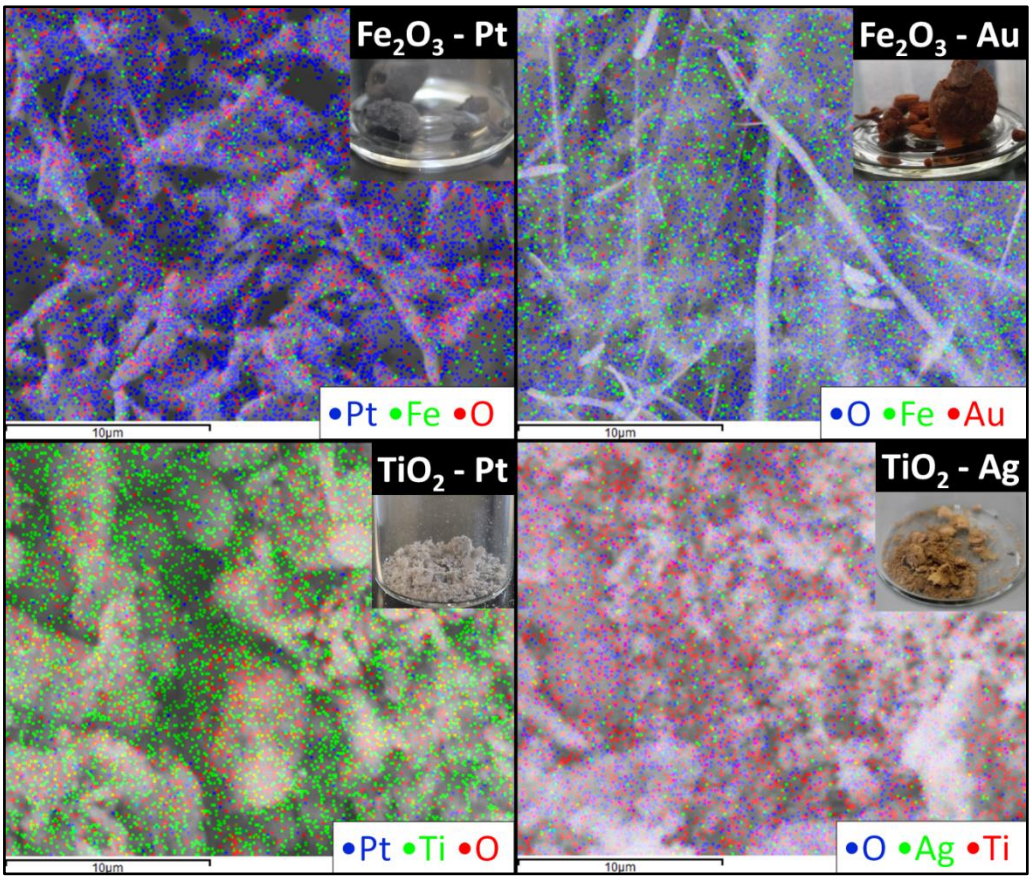

Figure S4. EDX mappings from SEM imaging of the cryoaerogel systems hematite-Pt, hematite-Au, TiO_2-Pt and TiO_2-Ag (always 1 wt% noble metal amount), revealing homogeneous distribution within the cryoaerogels at the respective magnifications chosen.

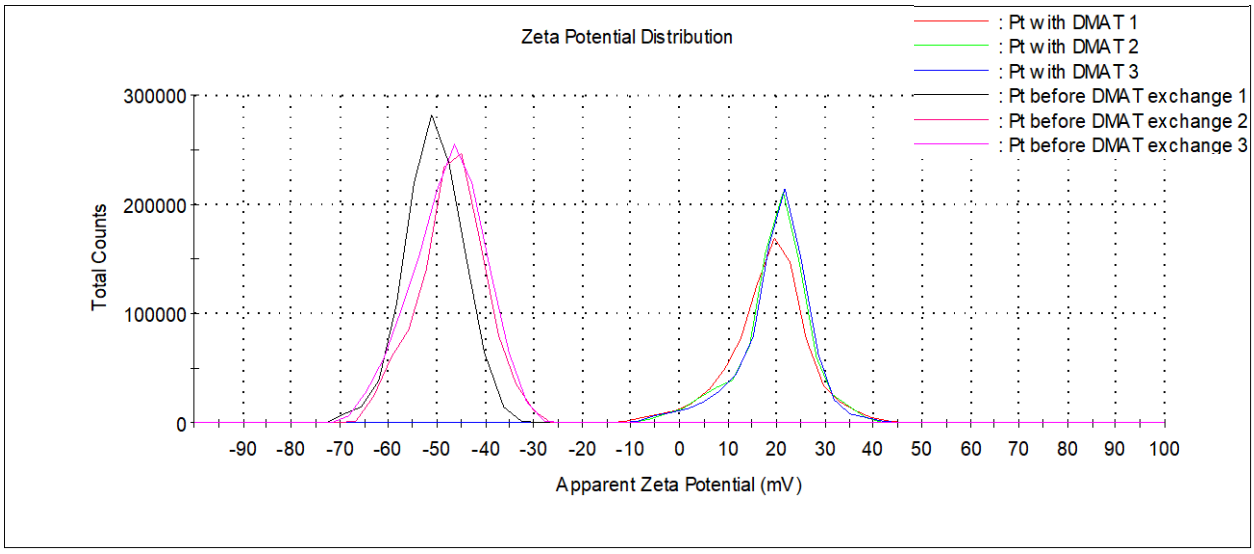

Figure S5. ζ-potential of the Pt nanoparticle solution before (labelled as Pt before DMAT) and after exchange of the surface ligands from citrate to DMAT (labelled as Pt with DMAT).

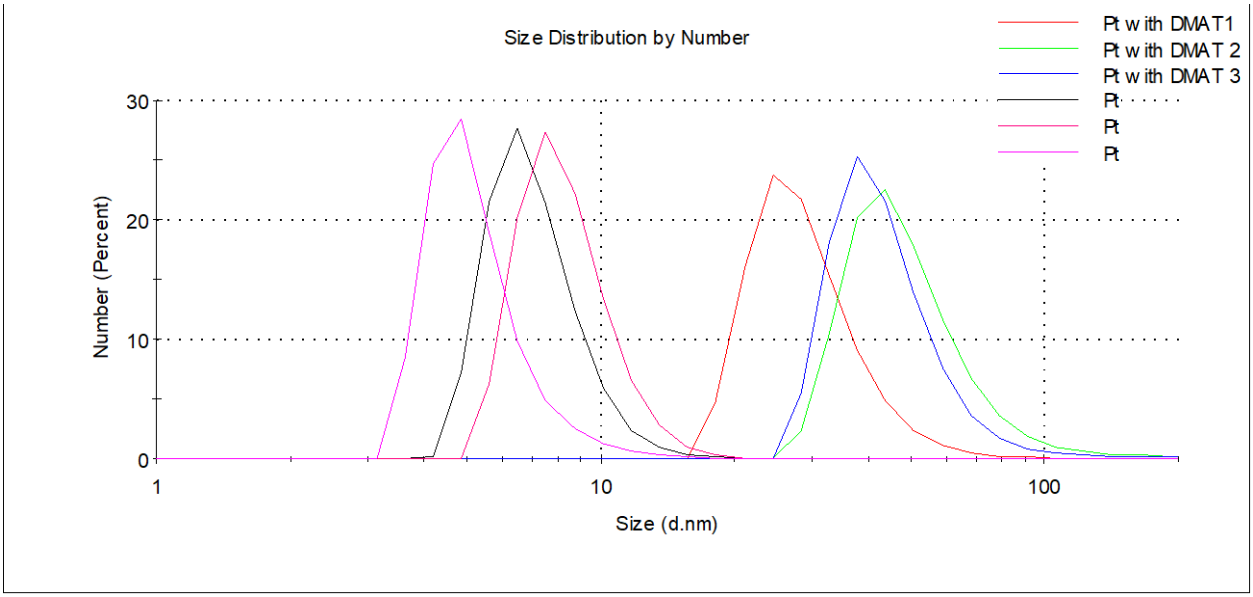

Figure S6. Size distribution measured by DLS for Pt nanoparticle solutions before and after ligand exchange to DMAT. The increase in size can be explained by the increased hydrodynamic radius of the particle and was not observed in TEM measurements.

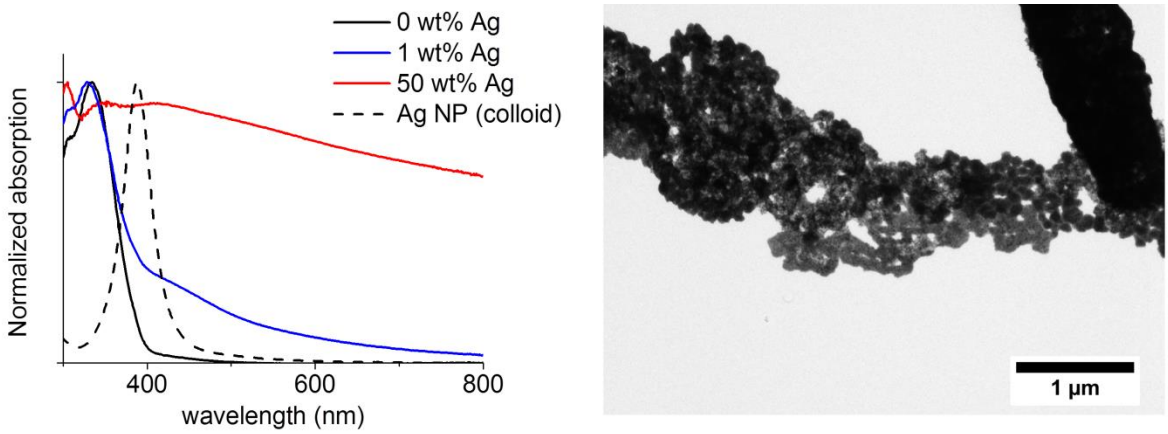

Figure S7. Normalized absorption spectra of TiO_2-Ag cryoaerogel films with varying composition ratios of 0 wt%, 1 wt%, 50 wt% Ag yield, and TEM image of the cryoaerogel with TiO_2-Ag (50 wt %) showing local segregation, due to Ag NP agglomerates, which were present already in solution.

Figure S6 shows the normalized absorption spectra of TiO_2-Ag systems with 0, 1 and 50 wt% of silver NP within the cryoaerogel. The increase of the amount of the optically active component (Ag nanoparticles), results in a more pronounced absorption maximum at 400 nm, which is caused by the localized surface plasmon resonance (LSPR) of silver nanoparticles. For the system with 1

wt% Ag, the absorption of the plasmon resonance is broadened compared to the colloidal NP. This effect may be caused by agglomerated silver particles or propagating plasmons.[1] In addition a bathochromic shift of the LSPR maxima can be observed, which is in part attributed to the change of the dielectric constant of the surrounding media (from water to titania), and in part to interplasmon interactions caused by aggregated Ag nanoparticles. For the 50 wt% Ag aerogel we additionally observe an extinction maximum at around 560 nm. This is probably related to the higher amount of silver and therefore the occurrence of interplasmon coupling.[2]

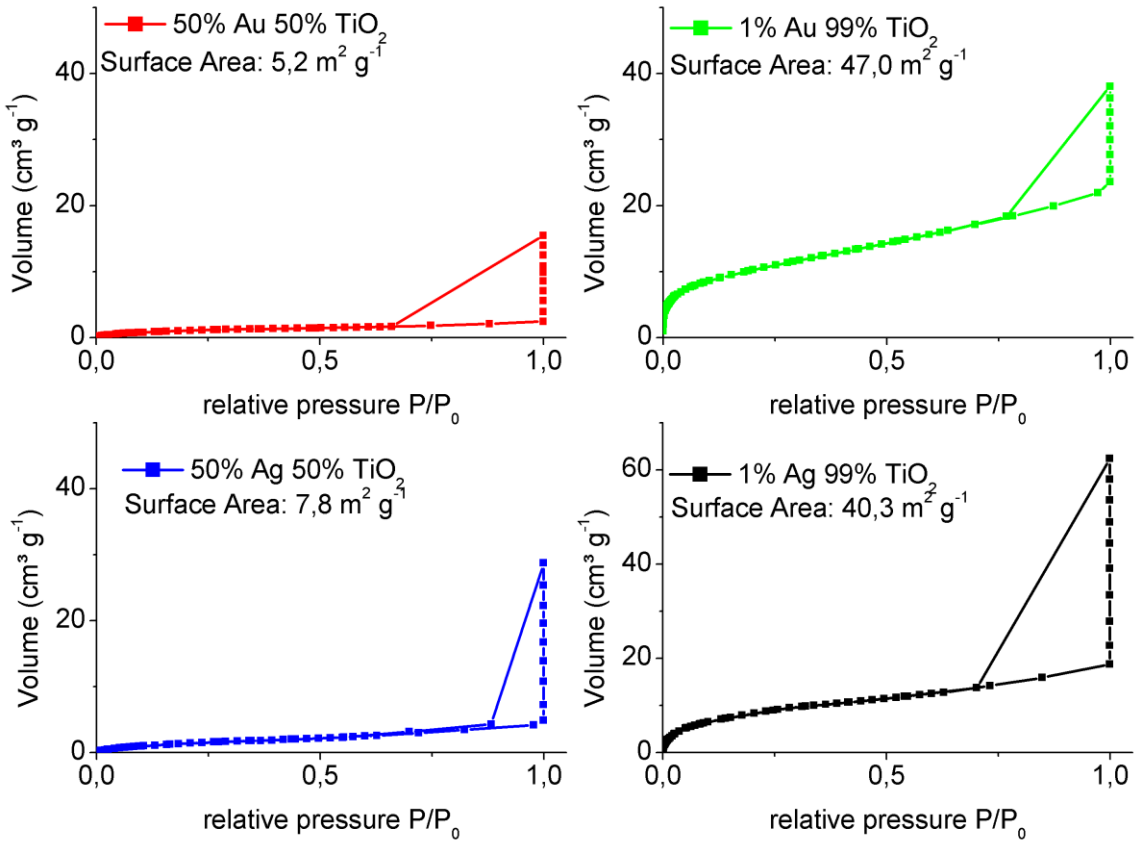

Figure S8. Krypton physisorption measurements of noble-metal titania cryoaerogels (Au and Ag). With larger noble metal contents, the specific surface area is decreased. The voluminous appearance of the corresponding macroscopic monoliths can be seen in figure S1 F and G.

Figure S9 shows the x-ray diffraction patterns of the Pt nanoparticles, and of the TiO_2 nanoparticles before gelation as well as of the mixed Pt-TiO_2 cryoaerogel with the composition 50% Pt nanoparticles and 50% TiO_2 nanoparticles. Similarly, Figure S10 shows the x-ray diffraction (XRD) pattern of the Au nanoparticles, of the TiO_2 nanoparticles and of the mixed Au-TiO_2 cryoaerogel with the composition 50% Au nanoparticles and 50% TiO_2 nanoparticles. Figure S11 shows the x-ray diffraction patterns of the Ag nanoparticles, TiO_2 nanoparticles and the mixed Ag-TiO_2 cryoaerogel with the composition 50% Ag nanoparticles and 50% TiO_2 nanoparticles. By comparing the recorded XRD pattern to literature, a mixture

of rutile and anatase phase can be determined for pristine TiO_2 nanoparticles. The pristine Pt nanoparticles, Au nanoparticles and Ag nanoparticles are present in the cubic phase. The crystal structure of the TiO_2 after cryogelation with Pt nanoparticles and Au nanoparticles was also determined as a mixture of anatase and rutile, which is marked via blue and red sign at the reflections. Blue labeled reflections only confirmed to the anatase phase, while red labeled reflections only confirmed to the rutile phase. From the XRD pattern of the mixed Ag-TiO2 cryoaerogel only the rutile phase can be determined. The observation of anatase is more complicated due to the overlaying Pt reflections at the positions of anatase (range 40 – 45° 2Theta). Besides, the resolution of the titania reflections is very less compared to the metal resolution. The phase of all metal nanoparticles are not affected by cryogelation and are all present in cubic phase.

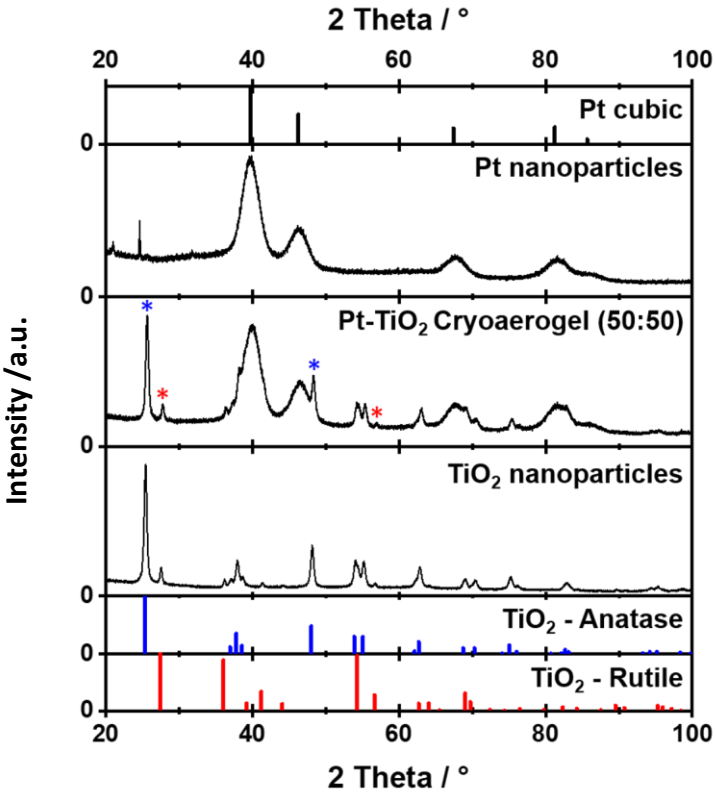

Figure S9. X-ray diffractograms of Pt nanoparticles, TiO_2 nanoparticles, and of the resulting mixed Pt-TiO_2 cryoaerogel. For comparison, the literature data for cubic Pt pattern (PDF card: 03-065-2868), TiO_2-Anatase pattern (PDF card: 03-065-5714) and TiO_2-Rutile pattern (PDF card: 01-070-7347) are shown as well.

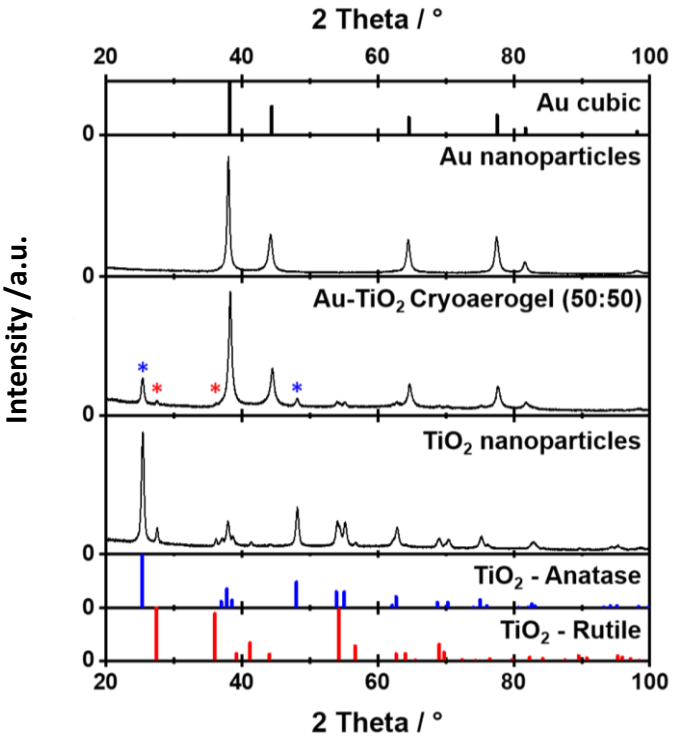

Figure S10. X-ray diffractograms of Aut nanoparticles, TiO_2 nanoparticles, and of the resulting mixed Au-TiO_2 cryoaerogel. Additionally, literature data for cubic Au pattern (PDF card: 00-004-0784), TiO_2-Anatase pattern (PDF card: 03-065-5714) and TiO_2-Rutile pattern (PDF card: 01-070-7347) are depicted.

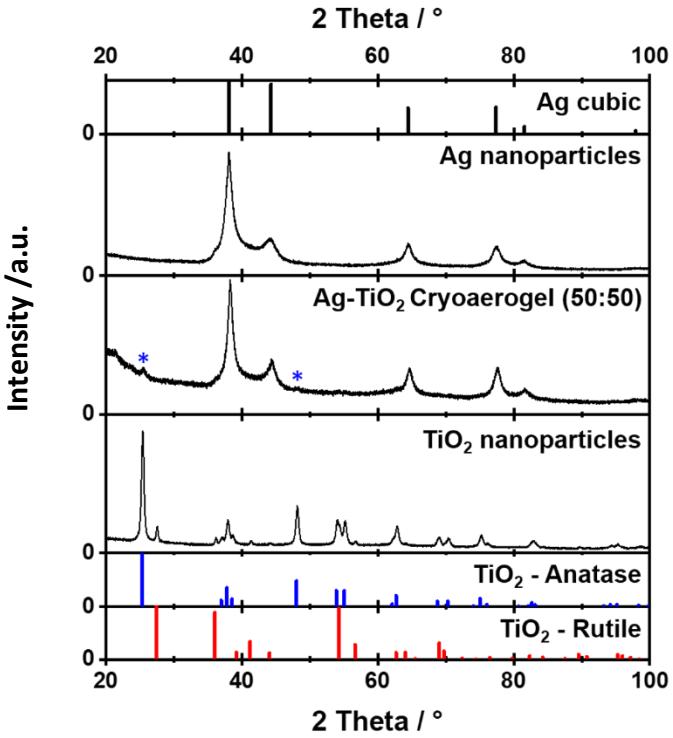

Figure S11. X-ray diffractograms of Ag nanoparticles, TiO_2 nanoparticles, and of the mixed Ag-TiO_2 cryoaerogel, as well as of the cubic Ag pattern (PDF card: 03-065-2871), TiO_2-Anatase pattern (PDF card: 03-065-5714) and TiO_2-Rutile pattern (PDF card: 01-070-7347).